atmosphere

MDPI

Article

Meteorological Drought Changes and Related Circulation Characteristics in Yulin City of the Northern Shaanxi from 1961 to 2015

Yixing Yin [1], Lijuan Zhang [2], Xiaojun Wang [3,4,*], Wucheng Xu [5], Wenjun Yu [1] and Ye Zhu [1]

1 School of Hydrology and Water Resources, Nanjing University of Information Science and Technology, Nanjing 210044, China; yinyx@nuist.edu.cn (Y.Y.); wj.yu@nuist.edu.cn (W.Y.); zhuye396@163.com (Y.Z.)
2 Tongren Meteorological Bureau of Guizhou Province, Tongren 554300, China; zlj0905@163.com
3 State Key Laboratory of Hydrology-Water Resources and Hydraulic Engineering, Nanjing Hydraulic Research Institute, Nanjing 210029, China
4 Research Center for Climate Change, Ministry of Water Resources, Nanjing 210029, China
5 School of Land and Resources, China West Normal University, Nanchong 637002, China; wucxu@126.com
* Correspondence: xjwang@nhri.cn; Tel.: +86-25-8582-8512

Received: 28 September 2020; Accepted: 2 November 2020; Published: 4 November 2020

check for updates

Abstract: This study explored the spatio-temporal patterns of meteorological drought change and the mechanisms of drought occurrence in Yulin City of the northern Shaanxi by using Standardized Precipitation Index (SPI), Empirical Orthogonal Function (EOF) analysis and composite analysis based on the meteorological observation data and NCEP/NCAR reanalysis data from 1961 to 2015. The main findings of the research are as follows: (1) In the annual and seasonal drought series, there is a non-significant trend toward drought in summer, while there are non-significant trends toward wetness for the other series. Overall, the frequency of drought is low in the southeast and high in the west and the north of the study area. (2) EOF1 is characterized by a uniform pattern in the whole region, i.e., there is a feature of consistent drought or flood in Yulin City. EOF2, EOF3 and EOF4 mainly indicate opposite characteristics of the changes of floods and droughts in the eastern/western parts and the southeast/other parts in the study area. (3) In the summer of the typical drought (flood) years, the study area is controlled by the northwest airflow behind the trough (zonal airflow at the bottom of low-pressure trough), and the meridional circulation (zonal circulation) is distributed in the mid-latitudes, which is conducive to the intrusion of cold air into the south (north) of China. The cold and warm air intersection area is to the south (to the north). The water vapor flux is weak (strong) and the water vapor divergence (convergence) prohibits (enhances) the precipitation process in the study area.

Keywords: meteorological drought; spatio-temporal pattern; circulation characteristics; northern Shaanxi; standardized precipitation index

1. Introduction

From a global perspective, drought is one of the most serious natural disasters, with the widest affected areas and the greatest economic losses [1–3]. China is a country with frequent droughts, and the drought disasters have great impacts on agriculture. In recent years, with the rapid development of society and economy, water shortages have occurred frequently, leading to more and more serious drought disasters [4–7]. In the context of global warming, the drought in northern China continues to intensify [8–10]. In northern Shaanxi, drought has developed into a major natural disaster, causing serious social and economic losses [11–15]. Therefore, it is of great significance to study the characteristics and mechanisms of the drought in northern Shaanxi [16,17].

There has already been an enormous amount of research on drought worldwide, and the research can be at the global scale [18–21], national and regional scales [22–25], and river basin levels [26–29]. Jehanzaib and Kim (2020) [30] summarized the current studies on drought risk analysis, forecasting and assessment under climate change. Sonh and Bae [31] investigated the changes in drought characteristics according to the shift in different climates from tropical, temperate, cold and polar to arid climate over the Asia monsoon region. Gocic and Trajkovic [32] explored the drought characteristics in the territory of Serbia and classified the study area into three sub-regions based on the drought identification. Li et al. [33] analyzed the spatio-temporal distribution and the anomalous characteristics of atmospheric circulation of the drought in the summer of 2006 in the eastern region of southwest China. Xu et al. [7] used a dry–wet index to analyze the spatio-temporal characteristics of autumn drought in southwest China during the period 1960–2009, and further investigated the atmospheric circulation characteristics based on National Centers for Environmental Prediction/National Center for Atmospheric Research (NCEP/NCAR) reanalysis data.

Drought indices are quantitative measures which can represent the level of drought by converting the data from one or several variables like precipitation and evapotranspiration into a single value [34]. A variety of drought indices are used at home and abroad to measure the degree of drought. Usually, drought indices include precipitation anomaly, Z index, composite meteorological drought index (CI), Standardized Precipitation Index (SPI) and Standardized Precipitation Evapotranspiration Index (SPEI), etc. Comprehensive reviews of drought indices can be found in [35,36]. Bao et al. [5] used the CI to analyze the occurrence frequency and the intensity of drought in Jiangsu Province in the past 50 years. Li et al. [13] improved the CI and tested the descriptive ability of the new CI index in the drought process in Shaanxi. Wang et al. [37] explored the spatio-temporal patterns of drought based on PDSI in the northwestern arid region of China during the period 1960 to 2010. Ayantobo et al. [38] made an investigation on the spatio-temporal changes in drought based on SPI, SPEI and CI at multiple timescales in China. Although there are some disadvantages and limitations for SPI (some of them include: (1) SPI uses only precipitation, and the estimation of water loss from evapotranspiration is not considered, (2) the use of different probability distributions affects the SPI values as is is based on the fitting of a distribution to precipitation series) [34,36], it is still widely used in drought studies [12]. Some of the most recent studies applying SPI indices in drought include [39–41].

The northern Shaanxi is located in the arid and semi-arid regions in China, and it also belongs to the agro-pastoral transitional zone. The area is sensitive to climate change and is ecologically and agriculturally fragile, and the annual precipitation is about the critical value of maintaining the ecology and crop growth in this area. The precipitation continues to increase in the northwestern part of China, forming the "dry in the east and wet in the west" character in northern China during the recent years [42,43]. Besides, located in the transitional region of the eastern humid area and western arid area, the northern Shaanxi is on the north edge of the summer monsoon, and thus it has a special atmospheric circulation background [44]. However, the circulation characteristics which lead to drought in the study area have not been fully understood to date.

This paper first investigates the spatio-temporal characteristics of meteorological drought change utilizing the drought index of SPI based on the daily precipitation data in Yulin City of the northern Shaanxi. Secondly, the Empirical Orthogonal Function (EOF) analysis is used on the summer SPI to reveal the spatio-temporal pattern of regional drought. Thirdly, according to the EOF result, the typical drought and flood years are selected and the NCEP/NCAR reanalysis data, including geopotential height field, wind field, vertical circulation, water vapor flux and water vapor flux divergence, are used to explore the circulation characteristics in the summer of typical drought and flood years, which can reveal the mechanism of drought in the region.

2. Data and Methods

2.1. Data

Yulin City is located in the northern part of Shaanxi Province with the geographical coordinates of 36°57′–39°35′ N, 107°28′–111°15′ E. The city has a maximum length of 309 km from the east to the west and a maximum width of 295 km from the north to the south, with a total area of 43,578 km^2, accounting for 21% of Shaanxi Province. The daily precipitation data of 12 meteorological stations in Yulin from 1961 to 2015 was selected, and the data are obtained from the National Meteorological Information Center of China Meteorological Administration. The National Meteorological Information Center has carried out strict quality control of the data. The quality control procedures mainly include correcting some suspicious/false observations, and correcting some data heterogeneity which may be caused by site migration and observation equipment upgrades. The study area and the spatial distribution of the meteorological stations are shown in Figure 1. The monthly NCEP/NCAR reanalysis data are used to analyze the circulation characteristics during the summer of typical drought and flood years. The selected elements included geopotential height, horizontal wind vector (including u and v components), vertical velocity (omega), surface pressure and specific humidity, and the horizontal grid spacing is 2.5° × 2.5°.

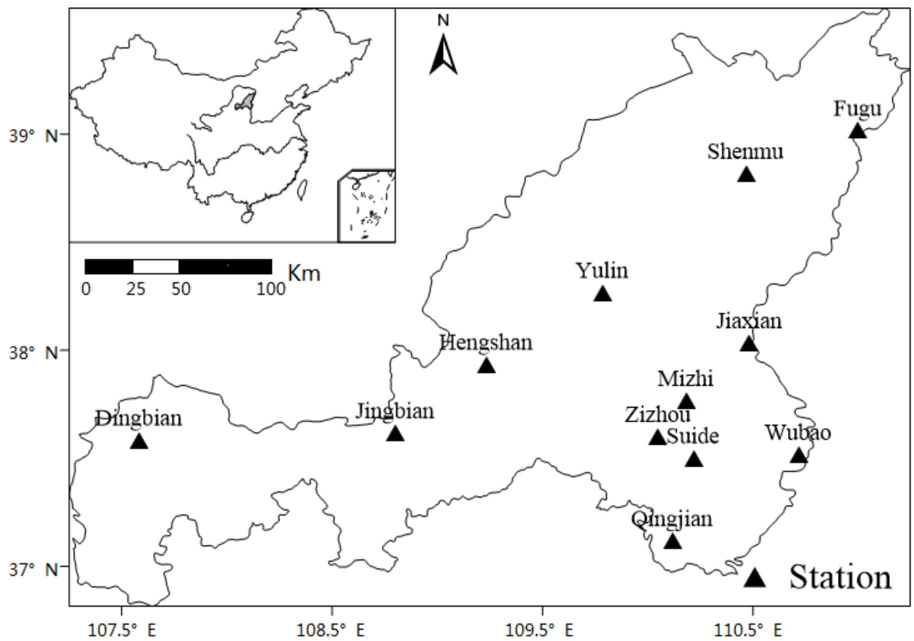

Figure 1. Spatial distribution of meteorological stations in Yulin City of the northern Shaanxi.

2.2. Methods

2.2.1. Standardized Precipitation Index

The Standardized Precipitation Index (SPI) is suitable for measuring drought characteristics. The advantages of SPI include the fact that the index assumes that the precipitation follows the Γ (Gamma) distribution, which not only takes into account that the precipitation itself follows the skewed distribution, but also applies normal standardization, so that it can reflect drought situation at different time scales and in different regions [14,45], and thus becomes another widely used drought index after the Palmer drought severity index [46,47]. The SPI index is calculated as follows.

Assuming that the precipitation in a certain period is a random variable x, the formula for calculating the probability density function of the Γ distribution is

$$f(x) = \frac{1}{\beta^{\gamma}\Gamma(x)}\, x^{\gamma-1}\, e^{-x/\beta} \quad (x > 0) \tag{1}$$

where $\beta > 0$ is the scale parameter; $\gamma > 0$ is the shape parameter; the formulas which are used to calculate the parameters β and γ are as follows

$$\hat{\gamma} = \frac{1 + \sqrt{1 + 4A/3}}{4A} \tag{2}$$

$$\hat{\beta} = \overline{x}/\hat{\gamma} \tag{3}$$

where

$$A = \ln \overline{x} - \frac{1}{n}\sum_{i=1}^{n} \ln x_i \tag{4}$$

where x_i is the observed precipitation data; $\overline{x}$ is the long-term average of precipitation; n is the length of the sequence.

As for the precipitation x_0 of a certain year, the probability of an event with a random variable x smaller than x_0 can be calculated after determining the various parameters above, which is

$$F(x < x_0) = \int_0^{\infty} f(x)dx \tag{5}$$

The probability of an event can be calculated using numerical integration. When the precipitation is zero, the probability of an event can be calculated by

$$F(x = 0) = m/n \tag{6}$$

where m is the number of observed values with a precipitation of 0; n is the total number of observed values.

Normal standardization is applied for the distribution probability of Γ, that is, the values obtained by Equations (5) and (6) are substituted into the standard normal distribution function

$$F(x < x_0) = \frac{1}{\sqrt{2\pi}} \int_0^{\infty} e^{-z^2/2} dx \tag{7}$$

An approximate solution to the formula above is

$$SPI = S\frac{t - (c_2 t + c_1)t + c_0}{((d_3 t + d_2)t + d_1)t + 1.0} \tag{8}$$

where $t = \sqrt{\ln \frac{1}{F^2}}$, $S = 1$ when $F > 0.5$; $S = -1$ when $F \leq 0.5$. The parameters are: $c_0 = 2.525517$, $c_1 = 0.802853$, $c_2 = 0.010328$; $d_1 = 1.432788$, $d_2 = 0.189269$, $d_3 = 0.001308$.

The value obtained by Equation (8) is SPI. Positive SPI values indicate that the precipitation is greater than the median while negative values indicate that the precipitation is less than the median. SPI is calculated at two kinds of time scale in this study: one is a 3-month scale, and the other is a 12-month scale. The 3-month scale is used for the estimation of seasonal drought and the 12-month scale is used for the estimation of annual drought.

2.2.2. Drought Occurrence Frequency

The "drought" part of SPI is divided into five grades in this paper, which are non-drought, mild drought, medium drought, severe drought, and extreme drought, and the corresponding SPI values are $-0.5 < SPI < 0$, $-1.0 < SPI \leq -0.5$, $-1.5 < SPI \leq -1.0$, $-2.0 < SPI \leq -1.5$ and $SPI \leq -2.0$, respectively. The occurrence frequency of drought at each station can be calculated by

$$P = \frac{n}{N} \times 100\% \tag{9}$$

where n is the number of the years when drought occurs, N is the length of data series. This paper contains precipitation data of 55 years, so N is 55.

2.2.3. Empirical Orthogonal Function

Empirical Orthogonal Function (EOF) is a method for analyzing the structural features of matrix data and extracting the main characteristics of data [48,49]. This method can decompose the time-varying variable fields into spatial functions that do not change with time and time functions that only depend on the time variation. The spatial functions summarize the spatial distribution characteristics of the fields, while the time functions are composed of linear combinations of the fields, also named the principal components. The first few principal components account for a large proportion of the total variance in the original variable fields, which are equivalent to concentrating the main information of the original fields on several main principal components. Thus, it is possible to replace the study of the temporal characters of the fields by the study of those of the principal components, and the results of EOF can be used to explain the physical characteristics of the variable fields. North test [50] and Monte Carlo test [51] are used to detect whether the modes are significant. For the detailed information of EOF method, please refer to [52].

The EOF method is to decompose the spatio-temporal data X into time vectors Z and space vectors V.

$$X = V \times Z \tag{10}$$

Among them, V is a matrix of n row and n column, where each column represents a typical space field. Z is an n-row and m-column matrix, and each row represents the time-weighted coefficients relevant to corresponding column in V. The space vectors are orthogonal to each other

$$V^T \times V = I \tag{11}$$

where I is a unit matrix. The time vectors are also orthogonal

$$Z \times Z^T = \Lambda \tag{12}$$

where Λ is a diagonal matrix. V and Z can be derived from the matrix X after defining the matrix A as follows

$$A = X \times X^T \tag{13}$$

The data will be processed as departure from the mean values of each station. Therefore, A is a covariance matrix and also a real matrix. According to the factorization theorem of real symmetric matrices, we have

$$A = V \times \Lambda \times V^T \tag{14}$$

where V is the eigenvector of A and also the space vector of X, Λ is the diagonal matrix of A whose principal diagonal is the eigenvalue of A and the rest are all 0. Then, the time vectors Z can be obtained as

$$Z = V^T \times X \tag{15}$$

3. Results and Analysis

3.1. Spatio-Temporal Changes in Drought

3.1.1. Changes in Annual and Seasonal SPI

Figure 2 shows the time series of the annual and seasonal SPI in Yulin City of northern Shaanxi. For seasonal time series, SPI is calculated by applying a moving average window of 3 months, and for annual time series, SPI is calculated by applying a moving window of 12 months. According to the annual series of SPI (Figure 2a), there is 1 year reaching the extreme drought grade, 1 year reaching the severe drought grade, 4 years belonging to medium drought, and 8 years belonging to mild drought during the period from 1961 to 2015. The annual SPI fluctuated greatly in the 1960s: it was the highest (severe flood) in 1964, while it was the lowest (severe drought) in 1965 during the study period. According to Wen and Zhai [53], the precipitation was very low (only 20–30 percent that of the normal years) from January to September in Yulin City in 1965, and flood disaster occurred in the whole province in 1964. From the 1970s to the beginning of the 21st century, there were frequent alternations between floods and droughts, but droughts were more evident. More droughts occurred from 1997 to 2006, with six drought years in 10 years. Similarly, Guo et al. [54] found that the droughts became more serious and frequent in Shaanxi Province after 1995. After 2007, drought was significantly relieved and more flood years occurred.

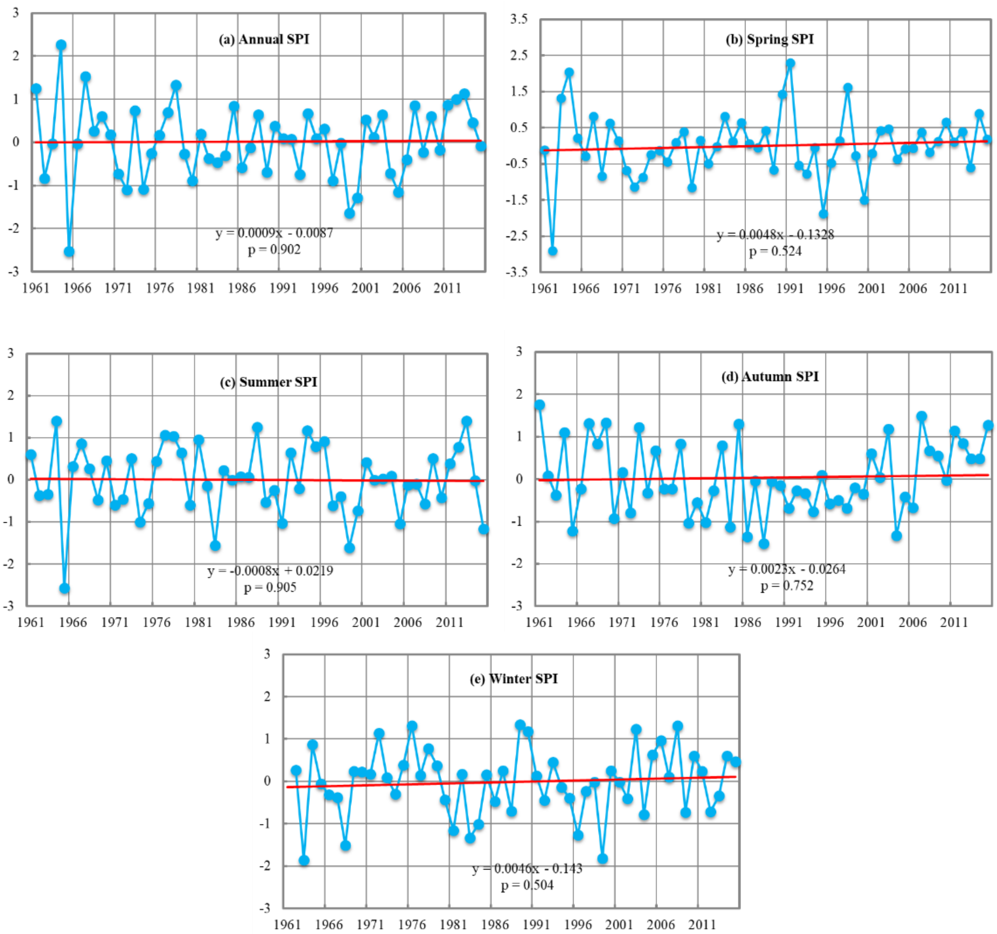

Figure 2. Variation characteristics of annual and seasonal standardized precipitation index (SPI) in Yulin City of the northern Shaanxi from 1961 to 2015. (**a**) Annual, (**b**) Spring, (**c**) Summer, (**d**) Autumn, (**e**) Winter.

It can be seen from Figure 2b–e that the most serious drought in spring occurred in 1962, with an SPI value of −2.89, reaching the extreme drought level; the most serious drought in summer occurred in 1965, with an SPI value of −2.57, reaching the extreme drought level; the most serious drought in autumn occurred in 1988, and its SPI value was −1.51, which reached the severe drought level; the most serious drought in winter occurred in 1963, and its SPI value was −1.85, which also reached the severe drought level. In addition, the occurrence numbers of mild drought, medium drought, severe drought and extreme drought in spring are 7, 3, 1 and 1, respectively; the occurrence numbers in summer are 7, 4, 2 and 1, respectively; the occurrence numbers in autumn are 9, 6, 1 and 0, respectively; the occurrence numbers in winter are 4, 4, 3 and 0, respectively. According to the fitting lines of the annual and seasonal series, there is a non-significant trend towards drought in summer, while there are non-significant trends toward wetness for the annual and the other seasonal series. Similarly, Guo et al. (2019) [54] found that the annual trend of droughts at four typical timescales is dominated by a decreasing trend in the Shaanxi Province. However, Jiang et al. (2019) [14] indicated that both the total number and the number of extreme/moderate drought months tend to increase from the 1951–1981 to 1982–2012 periods. This may be due to the different study periods. What's more, the number of meteorology stations of Jiang et al. (2019) [14] is very small (only five in the whole Shaanxi Province), which can lead to uncertainty in their results. This kind of mitigation of drought is consistent with the warming and humidification in the northwest of China [42,43].

3.1.2. Occurrence Frequency of Different Grades of Annual Drought

Table 1 summarizes the occurrence frequency of different grades of annual drought in the 13 stations over the years from 1961 to 2015. It can be seen that the total occurrence frequency of annual drought is the highest in Shenmu Station, reaching 37.05%, and the occurrence frequency of severe drought is also the highest; the total frequency of annual drought ranks the second in Jiaxian Station, reaching 36.91%, while the frequency of extreme drought ranks the first. When the total occurrence frequency of annual drought in a station is low, the frequency of the severe or extreme drought will also be high. The total frequency of annual drought is the lowest in Qingjian Station, which is 26.71%, but the frequency of mild drought is the second highest, and the frequency of extreme drought is the third highest. Overall, the frequency of total drought is between 26% and 38%, and 10 of the 12 stations have a total drought frequency of more than 30%.

Table 1. Occurrence frequency of different grades of annual drought in Yulin City.

Station	Mild Drought (%)	Medium Drought (%)	Severe Drought (%)	Extreme Drought (%)	Total (%)
Dingbian	12.73	13.73	6.45	0	34.91
Fugu	24.64	5.45	1.82	3.64	35.55
Hengshan	9.27	20.36	4.64	1.82	36.09
Jiaxian	21.18	10.09	0	5.64	36.91
Jingbian	18	4	8.6	4	34.6
Mizhi	13.04	8.7	9.27	0	31
Qingjian	21.22	1.64	1.02	3.04	26.71
Shenmu	10.1	11.99	12.97	1.99	37.05
Suide	21.22	6.17	2.14	1.02	30.55
Wubao	15.08	10.11	4.34	0	29.53
Yulin	15.73	15.91	1.82	2.82	36.28
Zizhou	17	11.33	1.22	1.22	30.77

3.1.3. Spatial Distribution of Annual and Seasonal Drought

Figure 3 shows the spatial distribution of the total occurrence frequency of annual and seasonal drought. It can be seen from Figure 3a that the spatial distribution of total drought frequency is high in the north and the west and low in the southeast for the annual series. The stations with a high frequency of occurrence of drought are mainly located in the western and the northern areas, and the stations with a low occurrence frequency appear in the southeast. The spatial patterns in the four seasons are generally similar to that of the annual series, except for winter. The spatial distribution of drought in winter (Figure 3e) is generally characterized by a high occurrence frequency in the north and a low occurrence frequency in the south and the west. Overall, the occurrence frequency of drought is mainly low in the southeast and high in the west and the north, and this is consistent with the precipitation distribution characteristics of abundance in the southeast and scarce in the northwest in the study area.

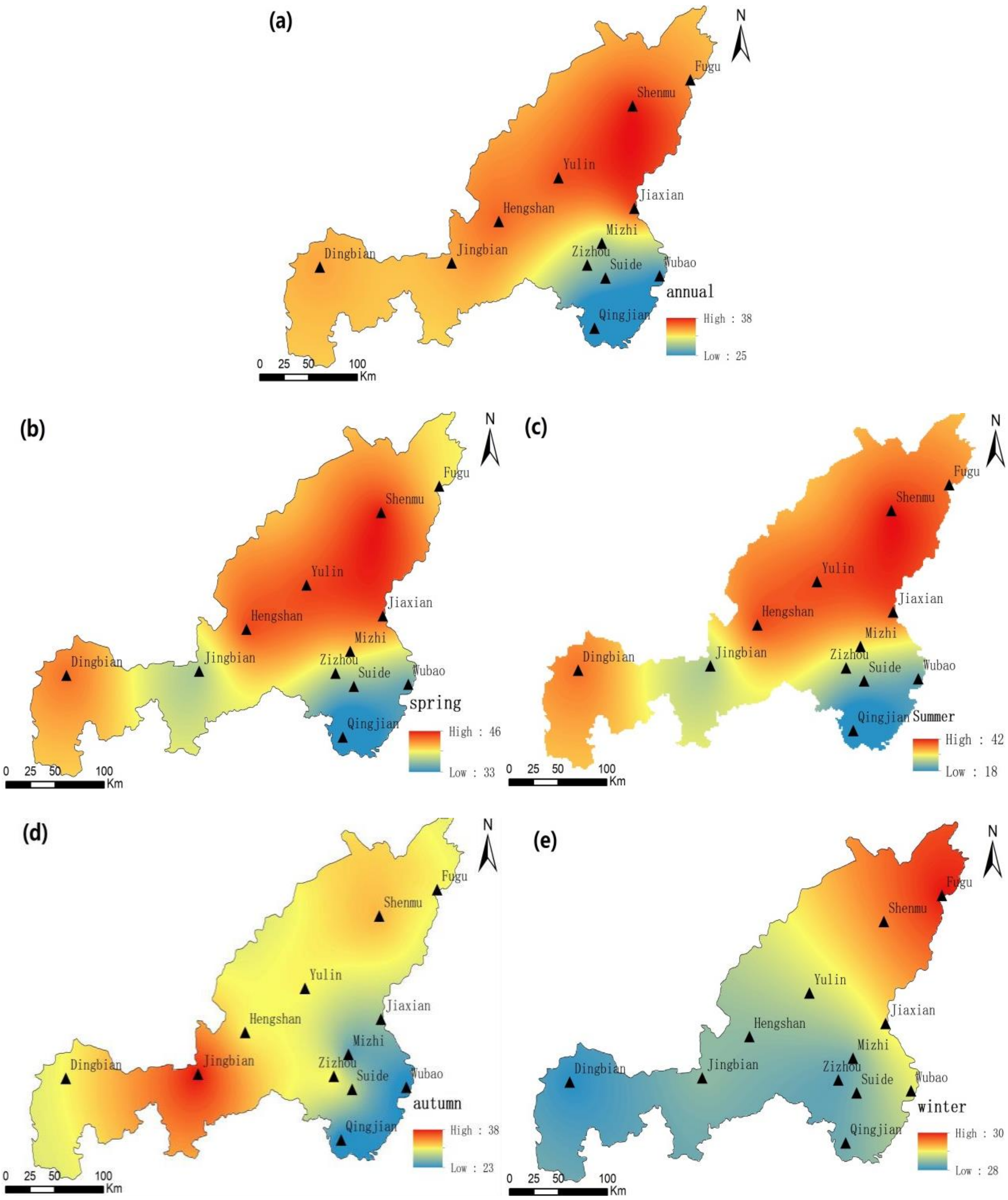

Figure 3. Spatial distribution of annual and seasonal total drought occurrence frequency (%) in Yulin City of northern Shaanxi. (**a**) Annual, (**b**) Spring, (**c**) Summer, (**d**) Autumn, (**e**) Winter.

What's more, the occurrence frequency is the highest in spring in the year. In spring, the range of occurrence frequency is between 33 and 46, i.e., both the upper and lower bounds are the highest in the annual and seasonal series. Similarly, according to Cai et al. [55], the drought frequency in each month is the highest in April and May (spring) and it is quite high in July (summer) and September (autumn) in Shaanxi Province. In summer, the stations in the northwest have the second highest drought frequency, while the stations in the southeast have the lowest drought frequency. The lower drought occurrence frequency in summer (in comparison to spring) may be due to the abundant summer precipitation in the study area. Most of the precipitation of the year occurs in summer, but the temperature is also high, which will increase the evapotranspiration, thus can lead to drought in summer. According to Cai et al. [55], the rainy season is from May to October in Shaanxi Province, and the drought frequency is also high in this period, indicating that drought and flood disasters coexist in the study area.

3.2. EOF Analysis of Summer SPI

Summer is the main rainfall season, and it is also the hottest season in China. Drought occurs mostly in summer, and the drought in summer attracts the most attention in China. Thus, we focused on the drought in summer, applied the EOF analysis to summer SPI, and investigated the circulation characteristics during typical summer drought in this paper. EOF analysis was used to analyze the summer drought in Yulin City. The results of North and Monte Carlo tests show that all the first four eigenvectors (EOF1, EOF2, EOF3, EOF4) pass the significance test. The cumulative variance contribution rate of the first four eigenvectors is about 83.7%, and the variance contribution rates are 57.6%, 12.6%, 7.9% and 5.6%, respectively. It can be seen from Figure 4a that EOF1 is characterized by a uniform positive pattern in the whole region, that is, there exists a feature of consistent drought or flood in Yulin City. Meanwhile, the values in the northern part are the highest, indicating that the changes in flood and drought are more obvious there. Figure 4b shows that EOF2 mainly exhibits a pattern of positive values in the southeast and negative values in the other areas, which implies that the changes in floods and droughts in the southeast are opposite to those in the other areas. In Figure 4c, EOF3 exhibits the opposite characteristics of the changes in floods and droughts in the eastern and western parts of the study area. In Figure 4d, similar to EOF2, EOF4 also mainly exhibits the opposite characteristics of the changes in floods and droughts in the southeastern part and the other regions. However, unlike EOF2, the low-value centers of EOF4 appear in the mid-western and mid-eastern regions. In general, it can be seen that the spatial distribution of drought occurrence frequency in Section 3.1.3 can be reflected by the second, third, and fourth modes of EOF analysis.

The principal components of the first four eigenvectors are shown in Figure 5. The product of a typical eigenvector and the corresponding principal component can reflect the spatial distribution of SPI changes in a certain year in the study area. The minimum value of PC1 (Figure 5a) occurred in 1965, indicating that it was generally the driest in Yulin City in the summer of 1965 (because EOF1 exhibits a uniform positive pattern); and the maximum of PC1 occurred in 1964, indicating that it was the wettest in Yulin City during the summer of 1964. This is consistent with the result of Figure 2c. The minimum value of PC2 (Figure 5b) appeared in 1967, indicating that the drought in the southeastern part of the study area was the most evident, while the flood in the rest of the area was the most evident (because EOF2 exhibits a pattern of positive in the southeast and negative in the other areas). The maximum appeared in 1965, indicating that the southeastern part of the year was the wettest, while the rest of the region was the driest. The linear trend of PC1 is positive, but not significant: the P value of the linear trend is only 0.779, and its MK trend value is only 0.41. Therefore, PC1 shows that the study area has a weak tendency toward wetness. PC2 and PC3 have a weak upward and downward trend, respectively. The linear downward trend of PC4 is significant, with a P value of 0.035, and the MK trend value is −1.87, significant at the 0.1 level.

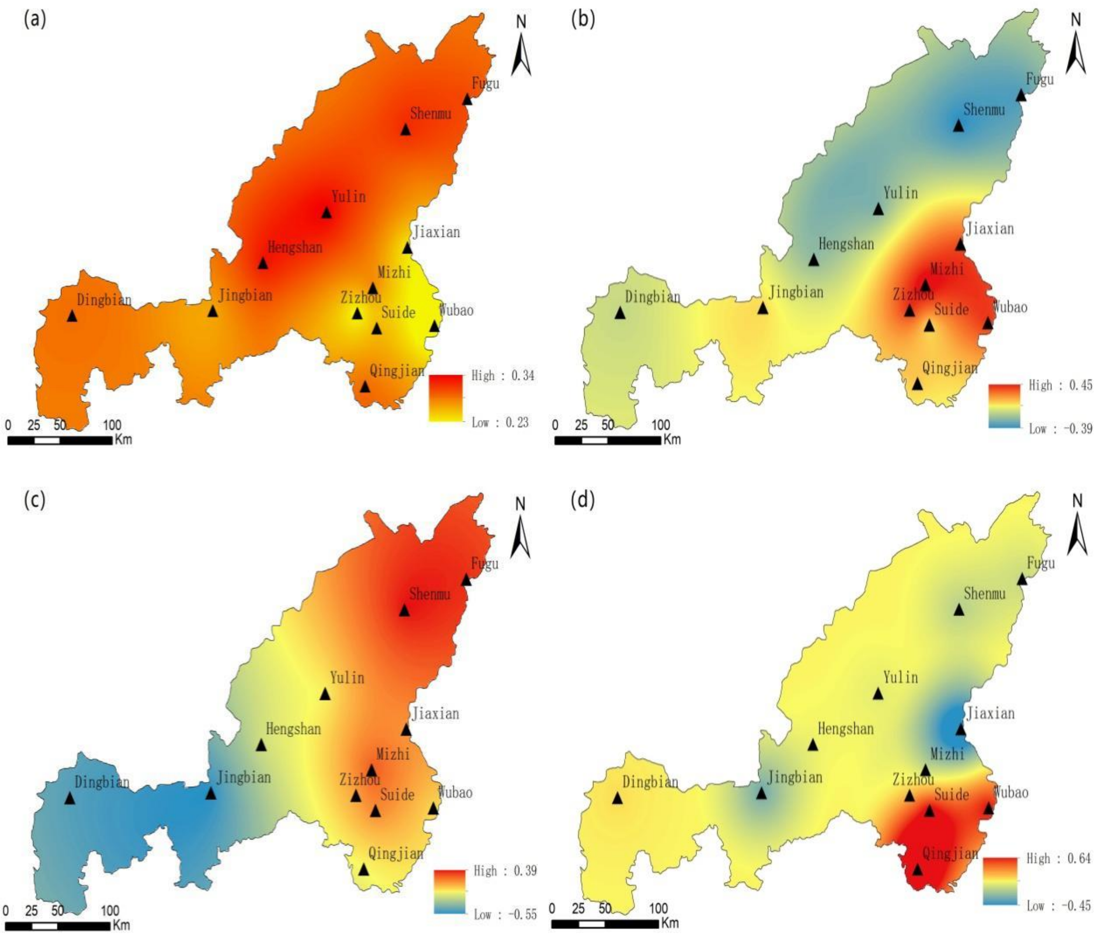

Figure 4. The first four eigenvectors of the Empirical Orthogonal Function (EOF) of the summer SPI from 1961 to 2015 in Yulin City of the northern Shaanxi. (**a**) EOF1, (**b**)EOF2, (**c**)EOF3, (**d**) EOF4.

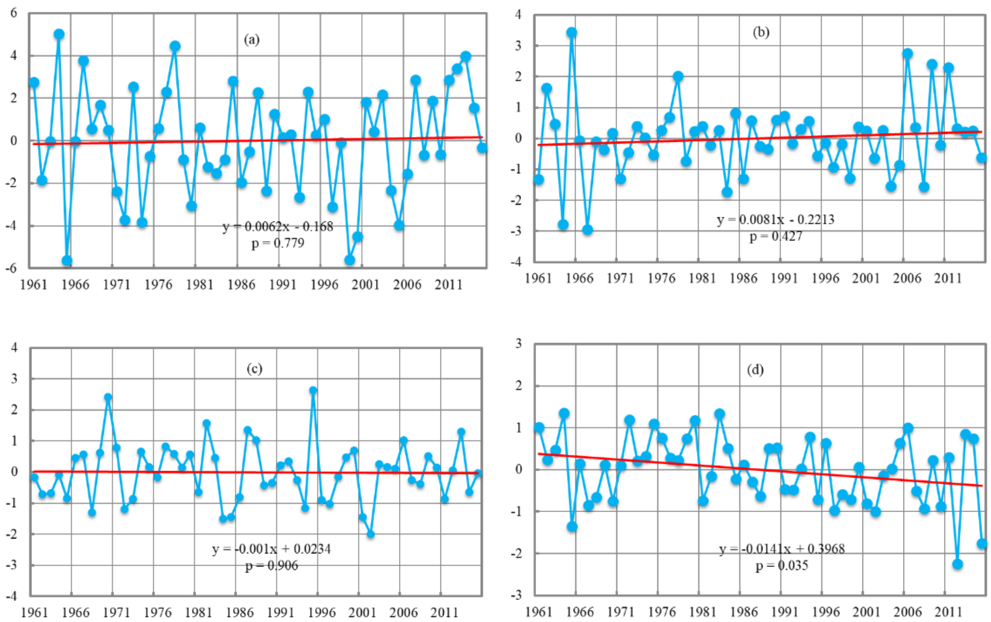

Figure 5. The first four principal components of the corresponding eigenvectors of the EOF analysis. (**a**) PC1, (**b**) PC2, (**c**) PC3, (**d**) PC4.

3.3. Circulation Characteristics in the Summer of Typical Years

The resolution of NCEP/NCAR reanalysis data is 2.5° × 2.5° which may not be fine enough for the relatively small study area. Although the study area is relatively small, the precipitation and drought in the region are determined by the circulation characteristics at the large scale which can be revealed by the NCEP/NCAR reanalysis data.

3.3.1. Selection of Typical Years

In this paper, the typical drought and flood years are selected based on the EOF analysis as follows: when PC1 is negative (positive) in a certain year, it is considered as a drought (flood) year. Moreover, if the absolute value of PC1 in that year is greater than the standard deviation of PC1, the year is further selected as a typical drought (flood) year. Finally, the typical drought years are determined to be 1965, 1974, 1983, 1999 and 2005, and the typical flood years are 1964, 1977, 1978, 1988 and 2013 in Yulin City of the northern Shaanxi.

3.3.2. Characteristics of Geopotential Height Field

Composite analysis of the summer 500 hPa geopotential height of the selected typical drought and flood years is shown in Figure 6. It can be seen from Figure 6a that the circulations in the mid-latitudes show a trough–ridge–trough pattern, and the study area is controlled by the northwest airflow behind the trough. Corresponding to the strong WPSH (West Pacific Sub-tropic High), the 5880 gpm characteristic line extends westward to 140° E. From the 500 hPa anomalous geopotential height field (Figure 6c), the Eurasian is characterized as "- + -", and there is a large range of negative anomalies with a closed center of −3 dagpm in China. The mid-latitudes show a meridional circulation distribution, which is conducive to the intrusion of cold air into the south of China, and the intersection area of cold and warm air is located in the south, which prohibits the formation of precipitation in Yulin City of the northern Shaanxi.

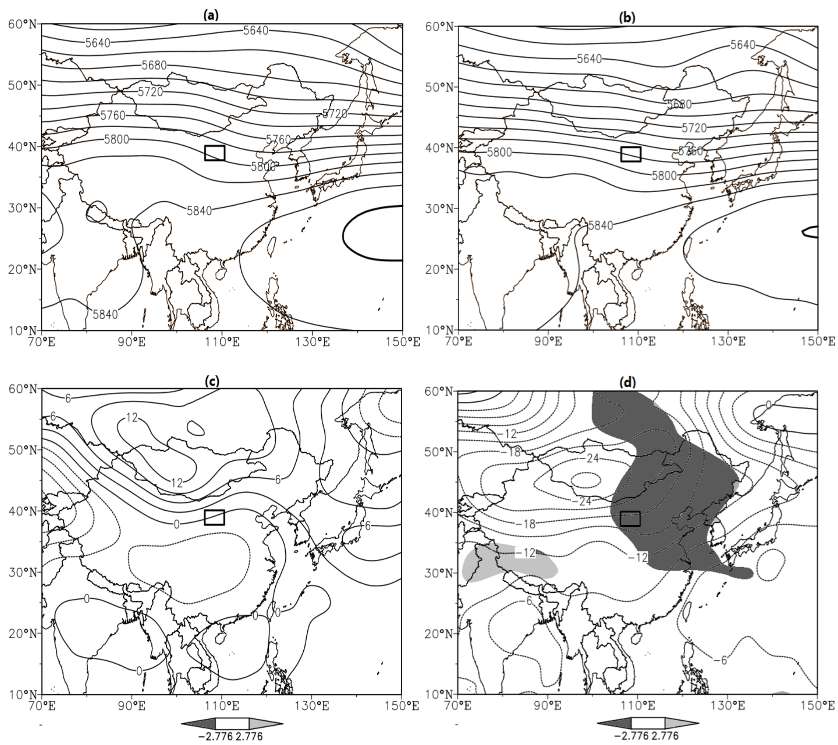

Note: The gray shaded areas indicate the area passing the 0.05 significance level test.

Figure 6. 500 hPa average geopotential height field (**a**,**b**) and anomalous geopotential height field (**c**,**d**) in the summer of the typical drought years (**a**,**c**) and flood years (**b**,**d**). (Unit: gpm).

In the 500 hPa geopotential height field of the summer of the typical flood years (Figure 6b), it can be seen that the mid-latitudes show a ridge–trough–ridge pattern, the northern Shaanxi is controlled by the zonal airflow at the bottom of the low-pressure trough, and the WPSH is weak. In the corresponding anomalous geopotential height field (Figure 6d), the mid-latitudes including the mainland China show negative anomalies, and it presents a zonal circulation distribution. The latitudinal airflow prevails throughout the mid-latitudes, thus the cold air is strong and lingers in the north of China. The warm and humid air is easy to move northward, and the intersection area of cold and warm air is to the north, which is conducive to precipitation in the northern Shaanxi.

3.3.3. Characteristics of Wind Field

Figure 7 shows the 850 hPa anomalous wind field in the summer of the typical drought and flood years. As can be seen from Figure 7a, in the typical drought years, the anomalous northerlies are in northeastern China, and the anomalous westerlies and easterlies are on the south and north sides of the Qinghai-Tibet Plateau, respectively. There are strong anomalous northerlies in southeastern China and there are cyclonic circulations near the eastern coast of China, which cause the rain belt to be in the southeast and prohibit the formation of precipitation in the study area. In the 850 hPa anomalous wind field of the flood years (Figure 7b), the anomalous southerlies present in the middle and eastern parts of China, and the anomalous easterlies and westerlies are on the south and north sides of the Qinghai-Tibet Plateau, respectively. Eastern China has strong anomalous southerlies, and there are anticyclonic circulations in the Jianghuai area to the vicinity of the Sea of Japan. The anomalous wind field is almost opposite to that of the typical drought years, causing the rain belt to be in the north, which is conducive to the formation of precipitation in the study area.

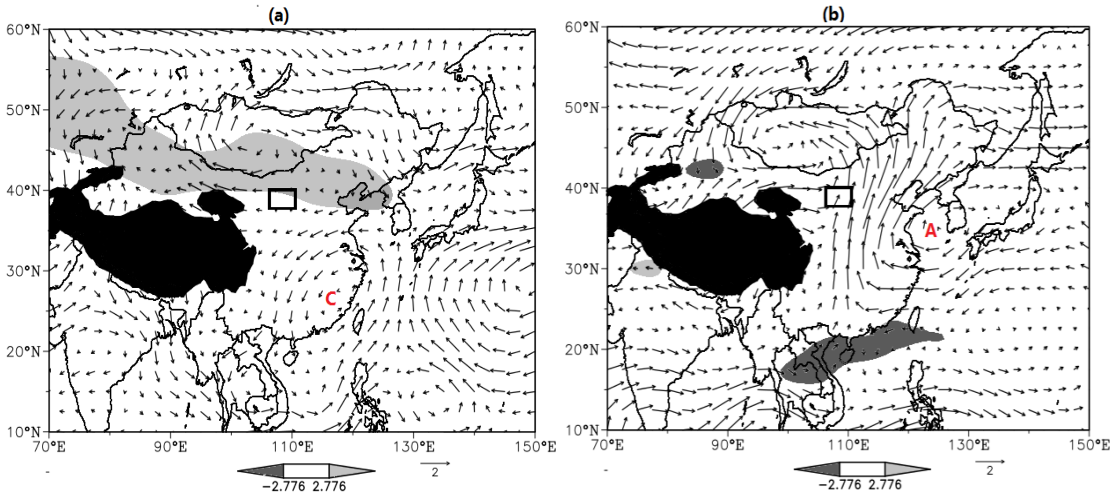

Figure 7. 850 hPa anomalous wind field (Unit: m·s^{-1}) in the summer of typical drought years (**a**) and flood years (**b**). The gray shaded areas indicate the area passing the 0.05 significance test. The heavy shaded area denotes the Qinghai-Tibet Plateau.

3.3.4. Characteristics of Vertical Circulation

Figure 8 shows the latitudinal-height profiles of average vertical circulations and the anomalies of vertical velocity during the summer of typical drought and flood years in the study area. As can be seen in Figure 8a, the study area (the rectangular area) is mainly controlled by the positive anomalies of vertical airflow (i.e., vertical upward movement is weakened) in the middle and lower troposphere in the typical drought years. The vertical ascending airflow is strong near the 300 hPa, and it is also very strong to the north of the study area. Therefore, the vertical upward transport of warm and humid air is restrained in the study area, which is unfavorable to the occurrence and development of precipitation, leading to drought in northern Shaanxi. In the typical flood years (Figure 8b), there is strong vertical upward movement from the lower to the upper troposphere over the study area compared with its north and south sides. The vertical ascending airflow from the lower to the upper troposphere is negative, and the minimum value appears near 700 hPa, indicating that the vertical upward movement is strong in the flood years, which is conducive to the occurrence of precipitation, leading to flood in northern Shaanxi.

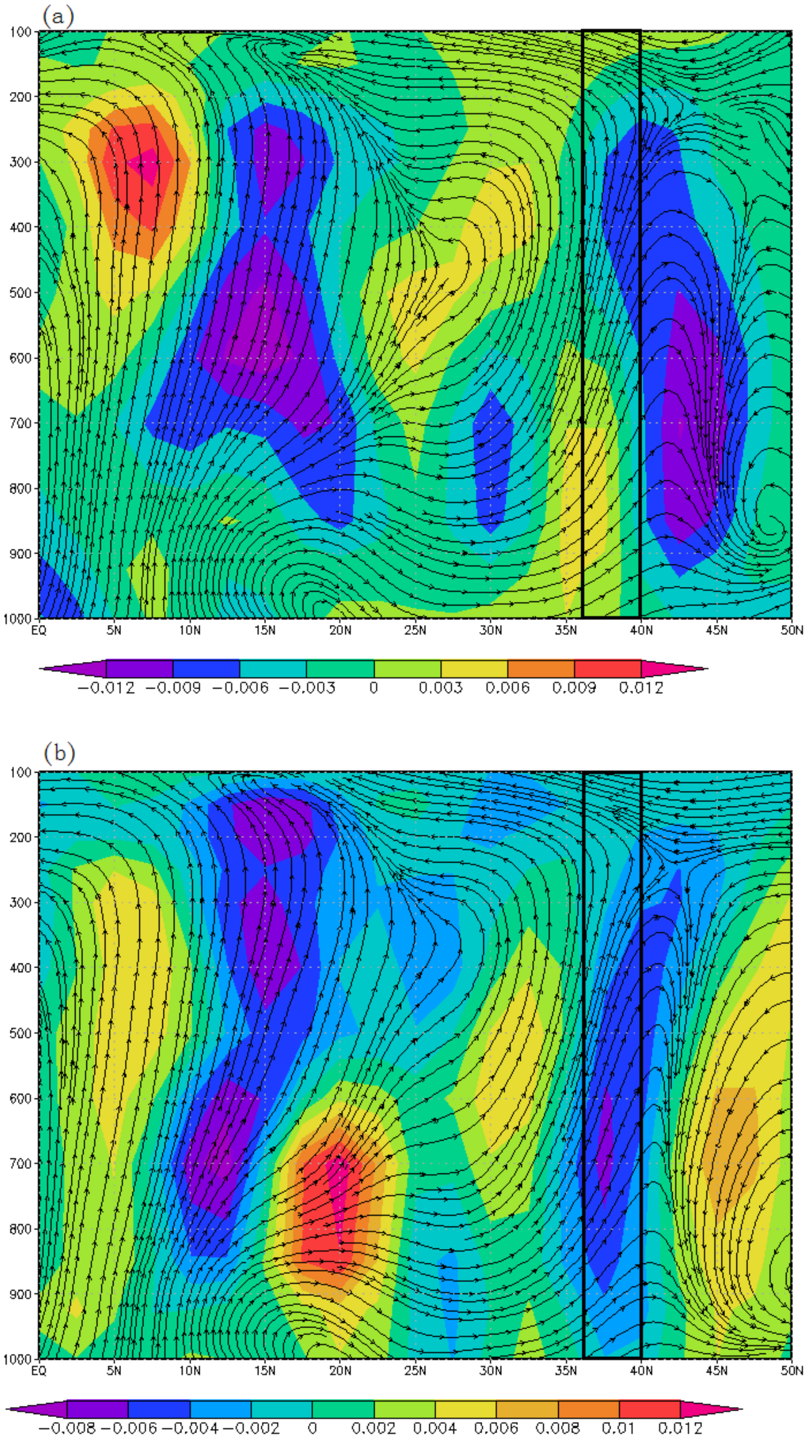

Figure 8. Average vertical circulations (streamlines) and anomalies of vertically velocity (shadows) in the summer of typical drought years (**a**) and flood years (**b**) within the longitudinal range from 106° E to 112° E. (Unit: Pa·s^{-1}). The vertical wind velocity streamlines are intensified by 100 times. The rectangular areas indicate the study area.

3.3.5. Characteristics of Water Vapor

From the water vapor flux anomalies in the summer of typical drought years (Figure 9a), the westward water vapor flux is negative in the northern Shaanxi, while there is a significant positive water vapor flux belt from the south of Japan to the southeast of China. The belt is located in the southeast of the study area and transports water vapor to the southeast coast of China. Therefore, the water vapor in the eastern and southeastern coastal areas is strong, while the water vapor in northern Shaanxi is weak. It can be seen from the water vapor flux anomalies of typical flood years (Figure 9b) that there are a large range of positive anomalies of water vapor flux in the northern, eastern and southern parts of China. According to the direction of water vapor transport, the water vapor is transported from the west to the east along the westerlies in the north. In the east, the water vapor is transported from the western Pacific Ocean to the eastern part of China, and turns from westward to northward in the eastern coastal region, which brings water vapor to northern Shaanxi and enhances the water vapor there.

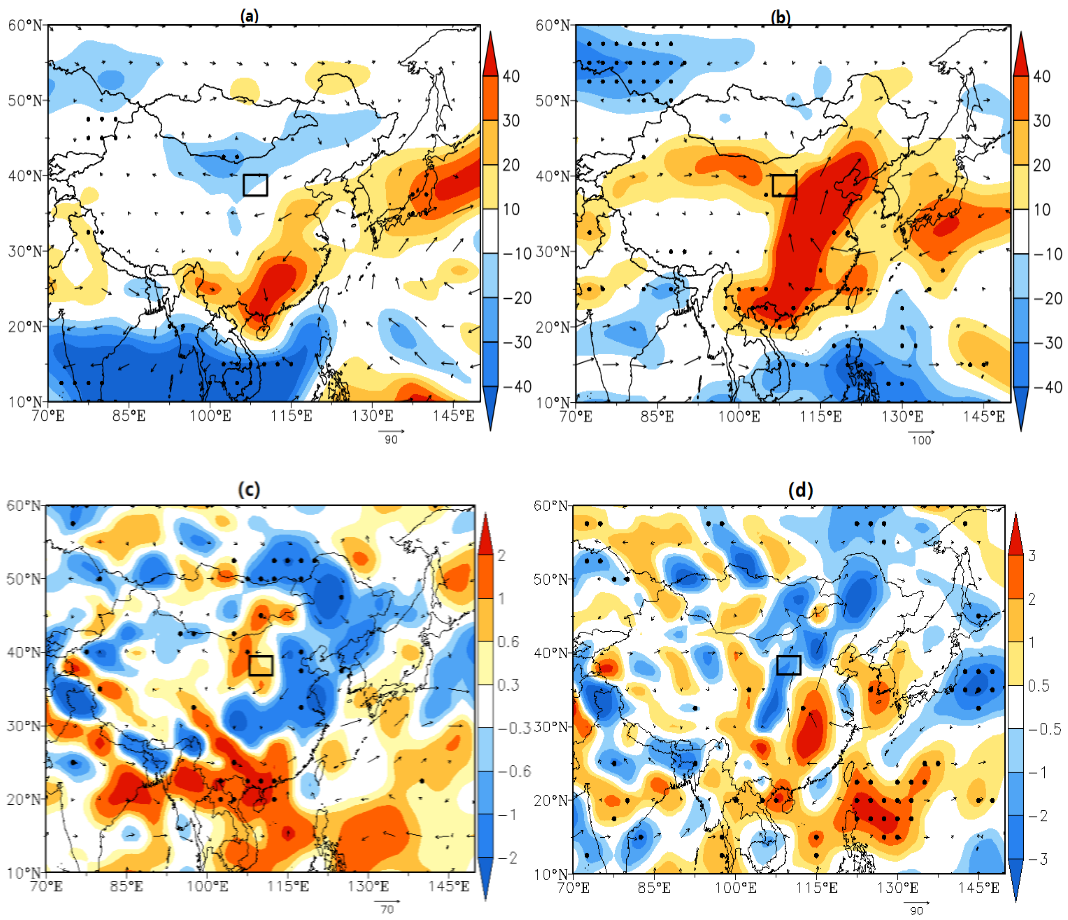

Figure 9. Integrated water vapor flux (Unit: kg·(m·s)$^{-1}$) (**a**,**b**) and water vapor flux divergence anomalies (Unit: 10^{-5} kg·(m^2·s)$^{-1}$) (**c**,**d**) in the summer of typical drought years (**a**,**c**) and flood years (**b**,**d**). The black points indicate the area passing the 0.05 significance test. The rectangular area indicates the study area.

From the water vapor flux divergence anomalies in the summer of typical drought years (Figure 9c), the study area exhibits positive values. The area is a moisture source, which is characterized by the divergence of water vapor, and the water vapor flux anomalies are negative (Figure 9a), thus the precipitation process is inhibited. In typical flood years (Figure 9d), the water vapor flux divergence anomalies are negative in northern Shaanxi. The area is a moisture sink, which is characterized by the convergence of water vapor, and the water vapor flux anomalies are positive (Figure 9b), which is beneficial to the occurrence of precipitation.

4. Conclusions

This study investigates the characteristics and changes of meteorological drought in Yulin City of the northern Shaanxi by using the SPI index, EOF analysis and composite analysis based on the meteorological observation data and NCEP/NCAR reanalysis data from 1961 to 2015. The study reveals the spatio-temporal patterns of drought change and the mechanisms of drought occurrence in the region, which can provide a reference for the early warning and prediction of regional drought. The conclusions are as follows:

(1) In the annual and seasonal drought series, there is a non-significant trend toward drought in summer, while there are non-significant trends toward wetness for the other series. Overall, the frequency of drought is low in the southeast and high in the west and the north of the study area;
(2) The results of EOF analysis of summer SPI show that EOF1 is characterized by a uniform pattern in the whole region, that is, there exists a feature of consistent drought or flood in Yulin City. EOF2, EOF3 and EOF4 mainly indicate opposite characteristics of the changes in floods and droughts in the eastern/western parts and the southeast/other parts of the study area;
(3) In the summer of the typical drought years, the study area is controlled by the northwest airflow behind the trough, and the meridional circulation is distributed in the mid-latitudes, which is conducive to the intrusion of cold air into the south of China. The cold and warm air intersection area is to the south. The water vapor flux is weak and the water vapor is divergent, which prohibits the precipitation process in the study area;
(4) In the summer of the typical flood years, the study area is controlled by the zonal airflow at the bottom of low-pressure trough, showing the distribution of zonal circulations, which is conducive to the intrusion of cold air into the north of China. The cold and warm air intersection area is to the north. The water vapor flux is strong and the water vapor is convergent, which is conducive to the precipitation process in the study area.

Author Contributions: Conceptualization, Y.Y.; funding acquisition, Y.Y. and X.W.; investigation, W.X.; methodology, Y.Y. and Y.Z.; resources, X.W., W.X. and W.Y.; software, L.Z.; supervision, Y.Y. and X.W.; visualization, L.Z.; writing—original draft, L.Z.; writing—review and editing, Y.Y. and X.W. All authors have read and agreed to the published version of the manuscript.

Funding: This research was funded by the National Key Research and Development Project (2018YFC1507704), the National Natural Science Foundation of China (51722905, 51911540477, 41961124006), Young Top-Notch Talent Support Program of National High-level Talents Special Support Plan and China Water Resource Conservation and Protection Project (126302001000150005).

Conflicts of Interest: The authors declare no conflict of interest.

References

1. Bruce, J.P. Natural disaster reduction and global change. *Bull. Am. Meteorol. Soc.* **1994**, *75*, 1831–1835. [CrossRef]
2. Obasi, G.O.P. WMO's role in the international decade for natural disaster reduction. *Bull. Am. Meteorol. Soc.* **1994**, *75*, 1655–1661. [CrossRef]
3. Kogan, F.N. Global drought watch from space. *Bull. Am. Meteorol. Soc.* **1997**, *78*, 621–636. [CrossRef]
4. Wu, Z.Y.; Lu, G.H.; Wen, L.; Lin, C.A. Reconstructing and analyzing China's fifty-nine year (1951–2009) drought history using hydrological model simulation. *Hydrol. Earth Syst. Sci.* **2011**, *15*, 2881–2894. [CrossRef]
5. Bao, Y.X.; Meng, C.L.; Shen, S.H.; Qiu, X.F.; Gao, P.; Liu, C. Temporal and spatial patterns of droughts for recent 50 years in Jiangsu based on meteorological drought composite index. *Acta Geogr. Sin.* **2011**, *66*, 599–608. (In Chinese) [CrossRef]

6. Niu, J.; Chen, J.; Sun, L. Exploration of drought evolution using numerical simulations over the Xijiang (West River) basin in South China. *J. Hydrol.* **2015**, *526*, 68–77. [CrossRef]
7. Xu, D.F.; Li, D.L.; Wang, H. Autumn dry-wet conditions and main types of atmospheric circulation in anomalous years in southwest China. *Chin. J. Atmos. Sci.* **2014**, *38*, 373–385. (In Chinese)
8. Qin, Y.; Yang, D.W.; Lei, H.M.; Xu, K.; Xu, X.Y. Comparative analysis of drought based on precipitation and soil moisture indices in Haihe basin of North China during the period of 1960–2010. *J. Hydrol.* **2015**, *526*, 55–67. [CrossRef]
9. Xu, Y.D.; Ren, C.Y.; Ma, X.D.; Zhao, D.N.; Chen, W. Change of drought at multiple temporal scales based on SPI/SPEI in Northeast China. *Arid. Zone Res.* **2017**, *34*, 1250–1262. (In Chinese)
10. Wang, X.Y.; Zhuo, L.; Li, C.; Engel, B.A.; Sun, S.K.; Wang, Y.B. Temporal and spatial evolution trends of drought in northern Shaanxi of China: 1960–2100. *Appl. Clim.* **2020**, *139*, 965–979. [CrossRef]
11. Xiao, J.; Zhao, J.B. The study on the characteristics of agricultural drought disasters in recent 54a in Shaanxi Province. *J. Arid Land Resour. Environ.* **2006**, *20*, 201–204. (In Chinese) [CrossRef]
12. Sun, Z.H.; Wang, Z.L.; Cao, X.M.; Yang, Q.; Liu, Z.C.; Lei, Y.P. Characteristics of drought change in the Loess Plateau Area of Shaanxi based on the standardized precipitation index during 1971–2010. *J. Desert Res.* **2013**, *33*, 1560–1567. (In Chinese)
13. Li, H.M.; Wang, Z.; Gao, M.S. The improved of comprehensive meteorological drought index and its application in Shaanxi Province. *Agric. Res. Arid Areas* **2015**, *33*, 260–266. (In Chinese)
14. Jiang, R.G.; Xie, J.C.; He, H.L.; Luo, J.G.; Zhu, J.W. Use of four drought indices for evaluating drought characteristics under climate change in Shaanxi, China: 1951–2012. *Nat. Hazards* **2015**, *75*, 2885–2903. [CrossRef]
15. Zhou, D.; Zhang, B.; Ren, P.; Zhang, C.; Yang, S.; Ji, D. Analysis of drought characteristics of shaanxi province in recent 50 years based on standardized precipitation evapotranspiration index. *J. Nat. Res.* **2014**, *29*, 677–688.
16. He, Y.; Zang, C.E.; Zang, L. Temporal and spatial characteristics of drought for recent 40 years in Shaanxi based on SPEI. *Shaanxi Meteorol.* **2014**, *5*, 26–32. (In Chinese)
17. He, Y.; Wang, Z.; He, H. Application of three dynamic drought-monitoring indexes in Shaanxi Province. Agricultural. *Res. Arid Areas* **2014**, *32*, 242–249, 274. (In Chinese)
18. Sheffield, J.; Wood, E.F. Characteristics of global and regional drought, 1950–2000: Analysis of soil moisture data from off-line simulation of the terrestrial hydrologic cycle. *J. Geophys. Res.* **2007**, *112*, D17115. [CrossRef]
19. Dai, A.G. Drought under global warming: A review. *Wiley Interdiscip. Rev. Clim. Chang.* **2010**, *2*, 45–65. [CrossRef]
20. Vicente-Serrano, S.M.; Beguería, S.; López-Moreno, J.I. A multiscalar drought index sensitive to global warming: The standardized precipitation evapotranspiration index. *J. Clim.* **2010**, *23*, 1696–1718. [CrossRef]
21. Van Lanen, H.A.J.; Wanders, N.; Tallaksen, L.M.; Van Loon, A.F. Hydrological drought across the world: Impact of climate and physical catchment structure. *Hydrol. Earth Syst. Sci.* **2013**, *17*, 1715–1732. [CrossRef]
22. Rajsekhar, D.; Singh, V.; Mishra, A. Hydrologic drought atlas for Texas. *J. Hydrol. Eng.* **2014**, *20*, 05014023. [CrossRef]
23. Hao, Z.; AghaKouchak, A. A nonparametric multivariate multi-index drought monitoring framework. *J. Hydrometeorol.* **2014**, *15*, 89–101. [CrossRef]
24. Houborg, R.; Rodell, M.; Li, B.; Reichle, R.; Zaitchik, B.F. Drought indicators based on model-assimilated Gravity Recovery and Climate Experiment (GRACE) terrestrial water storage observations. *Water Resour. Res.* **2012**, *48*, W07525. [CrossRef]
25. Wang, D.; Hejazi, M.; Cai, X.; Valocchi, A.J. Climate change impact on meteorological, agricultural, and hydrological drought in central Illinois. *Water Resour. Res.* **2011**, *47*, W09527. [CrossRef]
26. Tallaksen, L.M.; Hisdal, H.; van Lanen, H.A.J. Space-time modelling of catchment scale drought characteristics. *J. Hydrol.* **2009**, *375*, 363–372. [CrossRef]
27. Mishra, A.K.; Singh, V.P. Analysis of drought severity-area-frequency curves using a general circulation model and scenario uncertainty. *J. Geophys. Res. Atmos.* **2009**, *114*, D06120. [CrossRef]
28. Madadgar, S.; Moradkhani, H. Drought analysis under climate change using copula. *J. Hydrol. Eng.* **2013**, *18*, 746–759. [CrossRef]

29. Van Loon, A.F.; Tijdeman, E.; Wanders, N.; Van Lanen, H.A.J.; Teuling, A.J.; Uijlenhoet, R. How climate seasonality modifies drought duration and deficit. *J. Geophys. Res. Atmos.* **2014**, *119*, 4640–4656. [CrossRef]
30. Jehanzaib, M.; Kim, T.W. Exploring the influence of climate change-induced drought propagation on wetlands. *Ecol. Eng.* **2020**, *149*, 105799. [CrossRef]
31. Sonh, K.H.; Bae, D.H. Drought analysis according to shifting of climate zones to arid climate zone over Asia monsoon region. *J. Hydrol.* **2015**, *529*, 1021–1029. [CrossRef]
32. Gocic, M.; Trajkovic, S. Spatiotemporal characteristics of drought in Serbia. *J. Hydrol.* **2014**, *510*, 110–123. [CrossRef]
33. Li, Y.H.; Xu, H.M.; Liu, D. Features of the extremely severe drought in the east of Southwest China and anomalies of atmospheric circulation in summer 2006. *Acta Meteorol. Sin.* **2009**, *67*, 122–132. (In Chinese) [CrossRef]
34. Zargar, A.; Sadiq, R.; Naser, B.; Khan, F.I. A review of drought indices. *Environ. Rev.* **2011**, *19*, 333–349. [CrossRef]
35. Heim, R. A review of twentieth-century drought indices used in the United States. *Bull. Amer. Meteorol. Soc.* **2002**, *83*, 1149–1165. [CrossRef]
36. Mishra, A.K.; Singh, V.P. A review of drought concepts. *J. Hydrol.* **2010**, *391*, 202–216. [CrossRef]
37. Wang, H.J.; Chen, Y.N.; Pan, Y.P.; Li, W.H. Spatial and temporal variability of drought in the arid region of China and its relationships to teleconnection indices. *J. Hydrol.* **2015**, *523*, 283–296. [CrossRef]
38. Ayantobo, O.O.; Li, Y.; Song, S.B.; Yao, N. Spatial comparability of drought characteristics and related return periods in mainland China over 1961–2013. *J. Hydrol.* **2017**, *550*, 549–567. [CrossRef]
39. Kim, T.-W.; Jehanzaib, M. Drought Risk Analysis, Forecasting and Assessment under Climate Change. *Water* **2020**, *12*, 1862. [CrossRef]
40. Fang, W.; Huang, S.; Huang, Q.; Huang, G.; Wang, H.; Leng, G.; Wang, L.; Guo, Y. Probabilistic assessment of remote sensing-based terrestrial vegetation vulnerability to drought stress of the Loess Plateau in China. *Remote Sens. Environ.* **2019**, *232*, 111290. [CrossRef]
41. Mortuza, M.R.; Moges, E.; Demissie, Y.; Li, H.Y. Historical and future drought in Bangladesh using copula-based bivariate regional frequency analysis. *Theor. Appl. Climatol.* **2019**, *135*, 855–871. [CrossRef]
42. Ma, Z.G.; Fu, C.B. Interannual characteristics of the surface hydrological variables over the arid and semi-arid areas of northern China. *Glob. Planet. Chang.* **2003**, *37*, 189–200. [CrossRef]
43. Dai, X.G.; Wang, P.; Zhang, K.J. A study on precipitation trend and fluctuation mechanism in northwestern China over the past 60 years. *Acta Phys. Sin.* **2013**, *62*, 129201. (In Chinese)
44. Liu, X.Y.; Wang, J.S.; Li, D.L.; Yue, P.; Li, Y.H.; Yao, Y.B. Interannual and interdecadal atmospheric circulation anomalies of autumn dry/wet over the loess plateau and its multi-scalar correlation to SST. *Acta Phys. Sin.* **2013**, *62*, 219202. (In Chinese)
45. Tan, C.; Yang, J.; Li, M. Temporal-Spatial Variation of Drought Indicated by SPI and SPEI in Ningxia Hui Autonomous Region, China. *Atmosphere* **2015**, *6*, 1399–1421. [CrossRef]
46. Palmer, W.C. *Meteorological Drought*; Weather Bureau: Washington, DC, USA, 1965; pp. 45–58.
47. Alley, W.M. The Palmer Drought Severity Index: Limitations and Assumptions. *J. Appl. Meteorol. Clim.* **1984**, *23*, 1100–1109. [CrossRef]
48. Svensson, C. Empirical orthogonal function analysis of daily rainfall in the upper reaches of the Huai River basin, China. *Appl. Clim.* **1999**, *62*, 147–161. [CrossRef]
49. Smith, A.K.; Semazzi, H.M.F. The Role of the Dominant Modes of Precipitation Variability over Eastern Africa in Modulating the Hydrology of Lake Victoria. *Adv. Meteorol.* **2014**, *2014*, 11. [CrossRef]
50. North, G.R.; Bell, T.L.; Cahalan, R.F.; Moeng, F.J. Sampling errors in the estimation of empirical orthogonal functions. *Mon. Wea. Rev.* **1982**, *110*, 699–706. [CrossRef]
51. Peng, S.; Fyfe, J. The Coupled Patterns between Sea Level Pressure and Sea Surface Temperature in the Midlatitude North Atlantic. *J. Clim.* **2009**, *9*, 1824–1839. [CrossRef]
52. Yin, Y.X.; Pan, X.; Yang, X.Q.; Wang, X.J.; Wang, G.J.; Sun, S.L. Spatio-temporal changes and frequency analysis of multi-day extreme precipitation in the Huai River basin during 1960 to 2014. *Adv. Meteorol.* **2019**, *2019*, 6324878. [CrossRef]
53. Wen, K.; Zhai, W.Q. *China Meteorological Disaster Dictionary: Shaanxi Volume*; China Meteorological Press: Beijing, China, 2007.

54. Guo, M.; Li, J.; Wang, Y.; Long, Q.; Bai, P. Spatiotemporal Variations of Meteorological Droughts and the Assessments of Agricultural Drought Risk in a Typical Agricultural Province of China. *Atmosphere* **2019**, *10*, 542. [CrossRef]
55. Cai, X.L.; Li, Q.; Fang, J.G. Variation characteristics of regional meteorological drought events of Shaanxi Province. *Arid Land Geogr.* **2016**, *39*, 294–300. (In Chinese)